Thermoelectricity to power wireless sensors : an industrial appication

Vincent Boitier, Lionel Séguier, Bruno Estibals, Clément Arnaud, Thibault Anfrie, Cédric Maurin

THERMOELECTRICITY TO POWER WIRELESS SENSORS : AN INDUSTRIAL APPLICATION

V.Boitier[1], L. Seguier[1], B. Estibals[1], C. Arnaud[2], T. Anfrie[2] and C. Maurin[2]
[1] LAAS-CNRS, Université de Toulouse, CNRS, UPS, Toulouse, France,
[2]Arcelor Mittal, Fos Sur Mer, France

ABSTRACT

With permanently high temperature gradients, a steelwork is the ideal place to install thermoelectric generators (*TEG*). The electricity recovered is stored in supercapacitors and then conditioned to power a wireless communicating sensor (*a very energy-intensive lambda probe and its auxiliaries*). The particularity of the project lies in the unfavorable industrial environment (*high ambient temperature > 60°C, dust deposits, slag falls, etc.*), which complicates implementation and means that innovative solutions must be found.

KEYWORDS

Thermoelectric generator, TEG, Supercapacitors, Wireless Sensor, WSN, Energy Harvesting

INTRODUCTION

Improving industrial processes requires increased monitoring of installations, thanks to many judiciously placed sensors. This is particularly the case at Arcelor Mittal's coking plant in Fos/Mer, France. Measuring the oxygen content of the smoke boxes (*SB*) that collect the combustion fumes from the coking plant's ovens is important data for understanding and improving the quality of coke oven heating. This makes it possible to optimize and manage the firing of coal, thereby increasing the lifespan of the refractories and reducing the impact on the environment, since poor combustion leads to nitrogen oxide emissions.

In a large, complex industrial environment, the cost of a wired solution is prohibitive. Deploying a Lora antenna on the site enabled us to validate a wireless measurement transmission solution with a low rate of data packet loss.

The problem of energy supply remains to be solved. The electrical energy needed to power a wireless sensor usually comes from a battery located close to the communicating sensor. With an ambient temperature sometimes close to 60°C, a particularly energy-intensive sensor (*Lambda probe, 400J/cycle with a long 12V, 1.5A, 20s pre-heat*), and a desired measurement rate of less than 15 minutes, it is impossible to have several years' autonomy with a simple electrochemical accumulator.

As furnaces never stop, there is a permanent thermal gradient of over 50°C between the hot wall selected on a smoke box and the ambient air (*Fig. 1*). This makes it possible to use a Thermoelectric Generator (*TEG*), cf Part 1, which converts part of the heat flow into electricity to provide the necessary electrical power [1] [2]. This ambient energy recovery system is combined with a supercapacitors storage stage and control electronics, developed in Part 2. Part 3 shows some experimental results. Finally, the last part looks at the positives, the negatives and the outlook.

While it is easy to find commercial solutions for stand-alone power supplies based on photovoltaic energy, it is much rarer for solutions using thermal electro-generation. The work presented here could help users to develop their own applications more quickly.

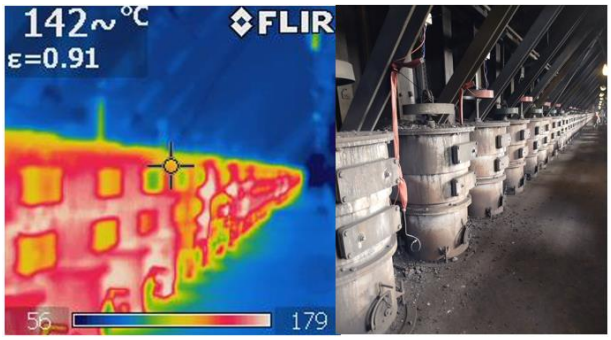

Figure 1. Thermal and visible image of a SB battery

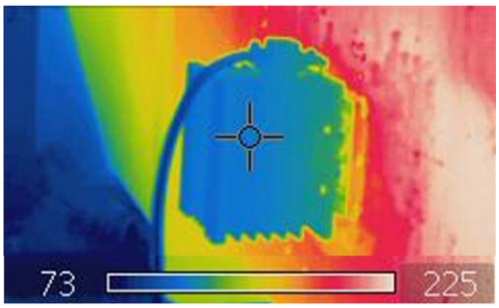

Figure 2. TEG+Heatsink installed on a Smoke Box

TEG BLOCK

Modeling

The thermal generator and heat sink assembly is shown in Fig. 2 and Fig. 3. The TEG is characterized electrically by its Seebeck coefficient *S* (*V/°C*) and its electrical resistance *R* (*Ω*). Standard electrical modelling gives the following electrical relationship:

$$V_{TEG} = S.\Delta T_{TEG} - R.I_{TEG} \qquad \text{Eq.1}$$

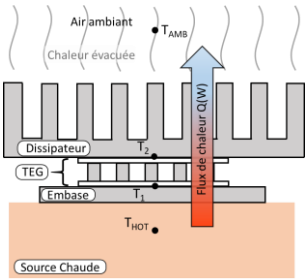

Figure 3. Modelling of the TEG + heatsink assembly.

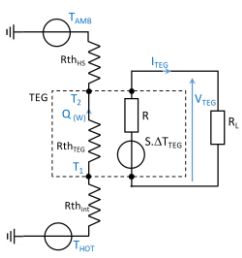

Figure 4.Thermal modelling by electrical analogy (according [3])

Thermally, the assembly is modelled with the simple model shown in Fig. 4 using an electrical analogy. With :

$$\Delta T = T_{HOT} - T_{AMB} \text{ and } \Delta T_{TEG} = T_1 - T_2$$

we obtain

$$\Delta T_{TEG} = \left(\frac{Rth_{TEG}}{Rth_{TEG}+Rth_{HS}+Rth_{int}}\right).\Delta T = \beta.\Delta T \quad \text{Eq.4}$$

This model allows an estimate of the electrical power that can be recovered as a function of the TEG and the heat sink chosen. [4] [5].

In practice, the uncertainties associated with heat exchange with the ambient environment (*ventilated or unventilated air, variations in the temperature of the hot spot, the temperature of the ambient air, etc.*) are significant. It is therefore not useful to have a more detailed model.

The open-circuit voltage at the terminals of the V_{OC} thermal generator is defined by the following relationship:

$$V_{OC} = S.\Delta T_{TEG} \quad \text{Eq.6}$$

The expression for the electrical power supplied by the TEG as a function of the TEG voltage is a parabola (cf laboratory tests with T_{AMB}= 25°C, T_{HOT} = 80°C : Fig. 5) with equation:

$$P_{TEG} = \frac{1}{R}(V_{OC} - V_{TEG}).V_{TEG} \quad \text{Eq.7}$$

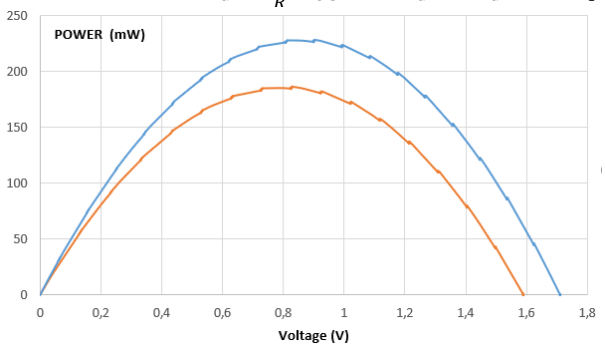

Figure 5. $P_{TEG}(V_{TEG})$, 5 minutes (blue) or 2 hours (orange) after fixing the system to the hot plate.

If the TEG flows over a matched equivalent impedance R_L (R_L= R), the electrical power is maximum and is equal to:

$$P_{MAX} = \frac{{V_{OC}}^2}{4.R} = \frac{(\alpha.\Delta T_{TEG})^2}{4.R} \quad \text{Eq.8}$$

The integrated circuit connected to the TEG will perform electrical impedance matching, setting V_{TEG} close to $V_{OC}/2$.

Simulation

The aim of the COMSOL simulations carried out is to estimate the effective thermal gradient across the TEG ΔT_{TEG} as a function of the overall thermal gradient ΔT between the hot wall and the ambient air. ΔT_{TEG} can then be used to predict the electrical power that can be recovered.

Simulation results (*see Fig.6*) show a significant temperature jump of around 15°C at the contact between the hot wall and the aluminum base of the TEG + heatsink assembly. This shows that particular care must be taken at this thermal contact to maximize ΔT_{TEG}.

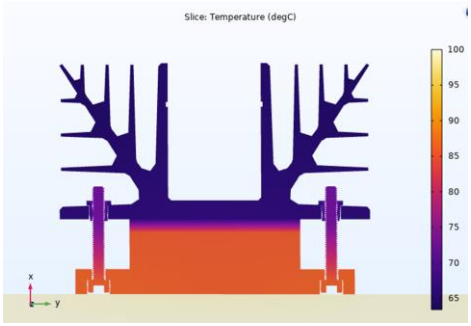

Figure 6. Comsol simulation with a 1.5cm thick base

More simply, the equivalent steady state electrothermal model also provides a reliable estimate of the actual gradient across the TEG for a given temperature difference between the hot wall and the ambient air. Typical values for careful contact give β between 0.3 and 0.4, 0.4 in our case.

$$\Delta T_{TEG} \approx 0{,}4.\Delta T \quad \text{Eq.9}$$

Technical implementation

The thermal generator chosen is a 5x5cm² TEconversion model, S = 0.0721V/°C, R between 3 and 5Ω. It can withstand high temperatures (*340°C permanently on the hot side*). It is combined with a heat sink featuring low thermal resistance (*1K/W*). The aluminimium base has 6 non-through holes. Magnets (*SmCo, T_{max} 200°C*) are positioned in these holes and wedged against the non-recessed part. The various parts are assembled using screws tightened to a constant torque (*4Nm*). Nylon screw insulators (T_{max} *160°C*) prevent thermal bridges between the screws and the heatsink. A thin layer of thermal grease is interposed between all parts in contact, except for the TEG, which is covered with a layer of graphite.

A 2-wire silicone cable was used to link the two units. It withstands temperatures ranging from -60 to +80°C.

A porcelain domino fixed to the heatsink provides the connections between the TEG and the cable to the electronics.

ELECTRONICS

Energy recovery and management

The power supply structure is shown in Fig. 7. Energy recovery is provided by an SPV1040 integrated circuit. It accepts a TEG voltage of between 0.3 and 5.5V. It incorporates a maximum power search function (*P&O type*). To protect the circuit, the 100kHz PWM blocks if the pix current reaches 1.8A or if the temperature reaches 155°C. This circuit is also protected against polarity inversion.

Storage is provided by 4 Maxwell supercapacitors of 100F, 2.6V each, mounted in 2S2P. They supply the 400J required to perform a complete measurement cycle.

Powered by the supercapacitors, a DC/DC step-up, built around an LT1619 PWM controller, supplies the 12V required by the load. The load consists of a Lambda sensor, a LoRa modem and control electronics (*not detailed here*).

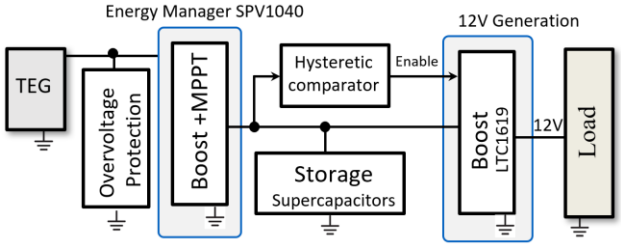

Figure 7. Power supply structure.

An output short-circuit protection (*STEF01*) is added at the 12V output. The whole unit should have been mounted in a box fixed to the fins of the heatsink (*Fig. 8*), but for safety reasons, all the electronics (*including sensor management and transmission*) have been integrated into a single box located in a less hot zone (T_{max}< *60°C instead of* T_{max}< *90°C*).

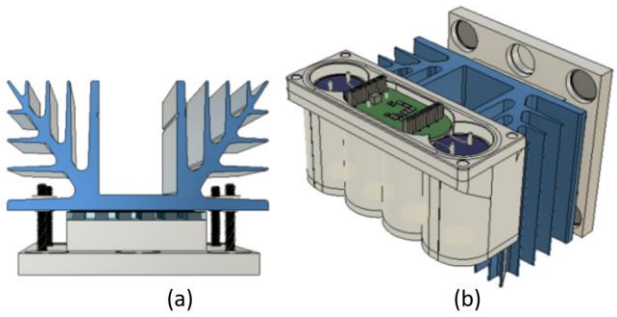

Figure 8. (a) heatsink / TEG assembly. (b) with storage stage and integrated control electronics.

Operation

As the initial charge of the supercapacitors can be very long (*cold-start phase*), a direct precharge with a table-top power supply is carried out the day before installation. The chosen precharge level enables the supercapacitors to be charged while the electronics are switched off (*power consumption remains limited to a few µA, thus preventing the supercapacitors from being discharged*).

Thanks to this precharge, the SPV1040 electronics start up a few seconds after the TEG is set, the supercapacitor voltage rises and reaches the comparator's toggle threshold, activating the 12V boost output stage. This powers a small auxiliary microcontroller which manages the measurement cycle (*Lora modem activation, Lambda probe preheating, O2 measurement, data transmission*). Between two measurement cycles, to minimize power consumption, the oxygen-measuring Lambda probe (*12V, 1A*) and the Lora modem (*12V, 10 mA*) are de-energized. The supercapacitors were discharged during the measurement cycle. Still powered up, the microcontroller wakes up and measures the supercapacitor voltage at regular intervals (*30s*). A new cycle starts as soon as the supercapacitors have recharged and reached a defined threshold. This ensures maximum measurement speed.

EXPERIMENTAL RESULTS

Fig. 9 shows 4 months of measurements. Two informations are given, The measurement rate and the thermal gradient ΔT between the T_{HOT} temperature measured with a thermocouple on the hot wall of the smoke box, close to the baseplate, and the T_{AMB} temperature measured with a thermocouple fixed 10 cm from the heat sink. We can see that the rate of measurement evolves inversely with the thermal gradient. Over the first 80 days, we also noted a slight increase in the time between two measurements, despite a similar thermal gradient. This may be due to clogging of the heat sink.

Fig. 10 shows the relationship between V_{SC} evolution and measurement rate. This gives a clear picture of the charge/discharge cycles of the supercapacitors. Data is transmitted each time the supercapacitors are discharged (black dot), which corresponds to the end of the measurement phase in the complete cycle.

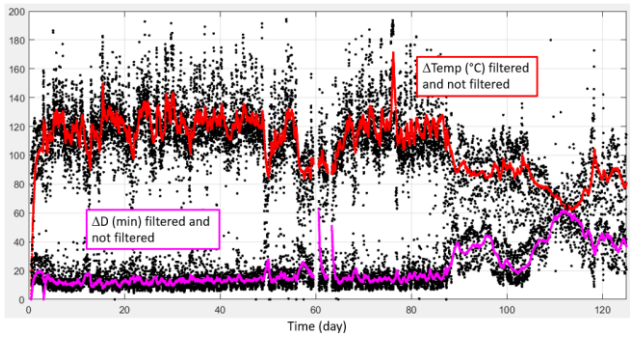

Figure 9. Measures from 20/02/2024.

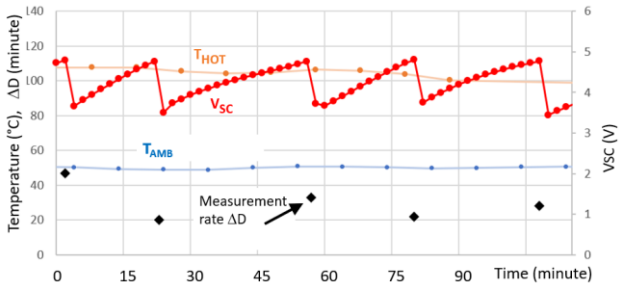

Figure 10. Cycling of supercapacitors (SC), with a measurement sent at the end of SC discharge.

Analysis of the supercapacitor charge curves enables us to determine the average stored power $<P_{SC}>$ from the relationship below.

$$< P_{SC} >= \frac{\Delta E_{SC}}{\Delta D} = \frac{(1/2).C(V_{SCmax}{}^2 - V_{SCmin}{}^2)}{\Delta D} \qquad \text{Eq.10}$$

A maximum value of 800mW is reached for a recharge time of 11 minutes with a gradient of 120°C. When the recharge time is close to an hour, the stored power remains just over 140mW at a gradient of 65°C.

Initially placed close to the ground in an area that was too hot, the electronics (*recovery, storage, modem*) were moved above the smoke boxes. The system is now fully operational. As far as Lora communication is concerned, there is a non-negligible rate of measurement loss, depending on the period *(ΔD is doubled if a measurement is lost*).

Analysis

First, the system installed is fully functional. The presence of a permanent thermal gradient, albeit variable according to the ambient air temperature and the operating phases of the SBs, is well suited to the use of thermal generation. We have validated the proper operation of the electronics up to +80°C (*laboratory measurements*). Electrical power recovery is optimal (*MPPT mode*) if the TEG voltage remains above 1V, which corresponds to a gradient of 35°C. This condition is always verified during normal coking plant operation.

The magnet fastening proved to be effective, but Experience has shown that, once the system has been positioned, inadvertent displacement of the TEG (*due to a person or piece of equipment bumping into the TEG*) drastically increases the thermal resistance of the soleplate/SB contact, which greatly degrades performance.

To avoid this, the TEG system has been positioned on the side of the SB rather than on the front (cf Fig. 11). Despite periods with T_{HOT} > 200°C (*beyond the recommended temperature for magnets*), the system remained fixed (*thermal grease hardens over time and acts like a glue*).

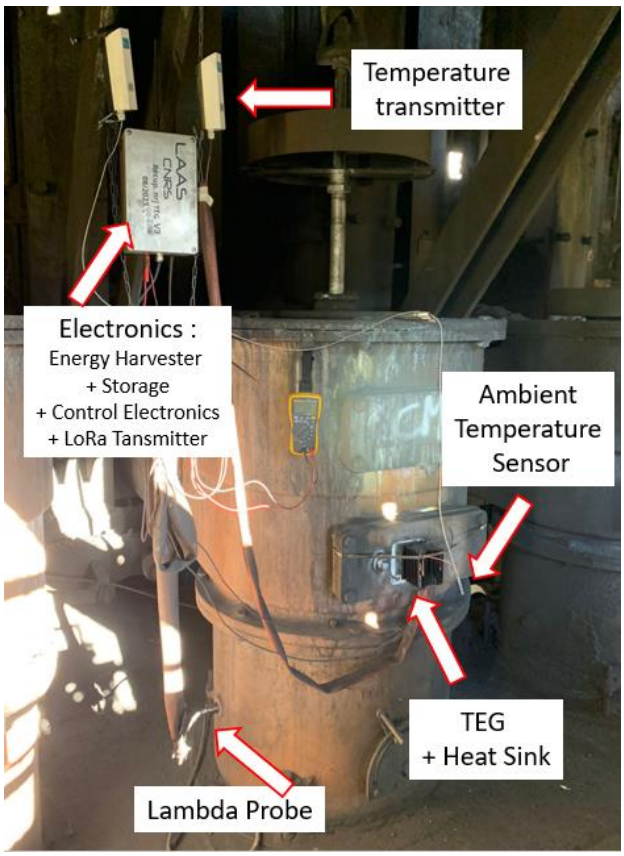

Figure 11. Instrumented SB. The electronics are offset to the top left (metal box), in a cooler area..

Weaknesses

This study showed the importance of contact between the hot wall and the TEG base to limit interface thermal resistance and thus maximize recoverable power. This makes surface preparation a crucial point, and one that is difficult to achieve on a surface that sometimes reaches 200°C. The thermal paste must also be deposited evenly. Once installed, the TEG must not be moved once the thermal paste has hardened. If the TEG has been moved, it is imperative to resurface the base and the hot wall before repositioning the TEG/dissipator assembly. If this is not done, the power recovered will be drastically reduced.

We also noted fouling of the TEG/Dissipator assembly, with no effect on the TEG, which is delivered encapsulated, but with a definite long-term effect on the heat dissipation provided by the fins.

Finally, it is worth noting the complexity of recovering the measurements required for on-site characterization in the industrial context of a coking plant (*need for authorization to go on site, difficulty in leaving fragile equipment on site, high ambient temperature, possible presence of gas, etc*.).

CONCLUSION AND OUTLOOK

We have shown that thermal generation offers a viable and effective solution for this type of application in difficult environments. Nevertheless, it is imperative to respect certain conditions of use to guarantee the system's performance.

For the remainder of this project, it will be interesting to work on the design of the heat sink to evacuate the heat flow as efficiently as possible. The question of fixing pressure also deserves to be studied to optimize the power recovered. A long-term study will also provide an answer to the question of the drop in performance caused by fin clogging.

It would also be interesting to have a compact one-piece solution, but unfortunately this is not possible when using a TEG to recover electrical power, unless the sensor is located in the same place as the TEG, which is quite rare. However, we intend to work on the thermal protection of the electronics to integrate TEG and electronics in a single block equivalent to a battery.

ACKNOWLEDGEMENTS

This work was carried out in collaboration with the Cokery Department and the Central Maintenance Department - EMAI | SCA3 of ArcelorMittal Méditerranée in Fos sur Mer.

REFERENCES

[1] H. Hachiuma et al., " Thermoelectric Generation Technology and the Applied Products", Komatsu technical report, 2019. https://home.komatsu/en/company/tech-innovation/report/pdf/190329_09e.pdf

[2] M.A. Zoui, S.Bentouba, J.G. Stocholm and M. Bourouis, « A Review on Thermoelectric Generators: Progress and Applications », Energies 2020, 13(14), 3606; https://doi.org/10.3390/en13143606

[3] D. Champier, « Thermoélectric generators : a review of applications », Energy Conversion and Management 140 (2017) 167–181, http://dx.doi.org/10.1016/j.enconman.2017.02.070

[4] M. Freunek, M. Müller, et al., "New physical model for thermoelectric generators" Journal of Electronic Materials, vol. 38, pp. 1214–1220, jul. 2009.

[5] R. Monthéard, "Récupération d'énergie aéroacoustique et thermique pour capteurs sans fil embarqués sur avion. ", thèse, 2014.